Computational Particle Mechanics (2022) 9:237–250
https://doi.org/10.1007/s40571-021-00406-0

Fully coupled meshfree numerical approach based on the finite pointset method for static linear thermoelasticity problems

Edgar O. Reséndiz-Flores[1] · Felix R. Saucedo-Zendejo[2] · Amaranta V. Jiménez-Villalpando[1]

Received: 3 January 2021 / Revised: 8 March 2021 / Accepted: 28 March 2021 / Published online: 10 April 2021
© OWZ 2021

Abstract

In this work, a promising fully coupled meshfree numerical approach is extended and implemented for the first time in the field of linear static thermoelasticity. A real meshfree method, the so-called finite pointset method (FPM), is applied and implemented in order to solve the strong/classical form of the governing partial differential equations for static linear thermoelasticity. Several benchmark problems are numerically solved in order to show the proposed coupled FPM numerical performance. The presented FPM meshfree approach shows excellent behavior for 2D linear static thermoelasticity problems even for complex geometries.

Keywords Linear thermoelasticity · Thermal expansion · Finite pointset method · Meshless method · Generalized finite difference method

List of symbols

A_i	PDE coefficient (·)
$\mathbf{B}$	PDE coefficient (·)
C_i	PDE coefficient (·)
E	Young's modulus Pa)
F	PDE coefficient (·)
G	Shear modulus (Pa)
J_1	Boundary conditions matrix (·)
J_2	Boundary conditions matrix (·)
J_3	Boundary conditions matrix (·)
K	Auxiliary matrix (·)
M	Differences matrix (·)
$\tilde{M}$	Block differences matrix (·)
Q	Auxiliary matrix (·)
T	Temperature (°C)
T_{ref}	Reference temperature (°C)
X	Set of nodes (·)
W	Weight matrix (·)
$\mathbf{a}$	Unknown vector (·)
$\mathbf{a}_\psi$	Unknown vector (·)
$\mathbf{a}_T$	Unknown vector (·)
$\mathbf{b}$	Unknown vector (·)
$\mathbf{e}_\infty$	Approximation error (·)
$\mathbf{f}$	Auxiliary vector (·)
h	Smoothing length (m)
$h_{i,k}$	Spatial differences (·)
k	Thermal conductivity ()
$\mathbf{n}$	Boundary normal vector (·)
$\mathbf{t}_0$	Surface traction (Pa/m)
$\mathbf{u}$	Displacement vector (m)
$\mathbf{u}_0$	Displacement at boundary (m)
w	Weight function (·)
$\mathbf{x}$	Arbitrary node position (m)
$\mathbf{x}_i$	ith node position (m)
Γ_d	Dirichlet boundary (·)
Γ_n	Neumann boundary (·)
Γ_r	Robin boundary (·)
$\widetilde{\Psi}$	Unknown vector (·)
Ω	A given fluid domain (·)
α	Weight function parameter (·)
β	Thermoelastic coefficient (Pa °C^{-1})
ψ	Field variable (·)
ψ_j	jth unknown component (·)
γ	Coefficient of thermal expansion (°C^{-1})
δ	Perturbation magnitude (·)
λ	Lame's first parameter (Pa)

✉ Felix R. Saucedo-Zendejo
fesaucedoz@uadec.edu.mx

1 División de Estudios de Posgrado e Investigación, Tecnológico Nacional de México/IT de Saltillo, Blvd. V. Carranza 2400, Col. Tecnológico, C.P. 25280 Saltillo, Mexico

2 Centro de Investigación en Matemáticas Aplicadas, Universidad Autónoma de Coahuila, Camporredondo S/N, C.P. 25115 Saltillo, Mexico

μ	Lame's second parameter (Pa)
ν	Poisson's ratio $(\cdot)$
σ	Stress tensor (Pa)
ε	Strain tensor (Pa)
σ_{ij}	Stress component (Pa)
σ_v	von Mises stress (Pa)
φ	Boundary condition value $(\cdot)$
Δ	Laplace operator (m^{-2})
∇	Gradient operator (m^{-1})

1 Introduction

Static linear thermoelastic problems take place in different applications in engineering. Different works have been carried out to numerically model thermomechanical phenomena, such as forging [4], fatigue [12], welding [11] and solidification of steel [24]. Finite element method is a common method used in these works [33]. However, practical guidelines for dealing with large-scale problems involving several variables are still missing and efforts have been made to overcome computational limitations in the finite element method [9]; in spite of this, meshfree methods have also been developed to overcome these limitations, such as the simulation of complex geometries and difficulties for remeshing.

Meshless methods can be classified in terms of the partial differential equation (PDE) form, namely weak form and strong form meshless methods [27]. In terms of weak form methods, it can be said that one of the most used weak form meshless method is the elementfree Galerkin method (EFG). It has been reported that this method can be used to analyze plates under mechanical loading as well as thermal gradient [7] and solving edge crack problems with the effect of crack interactions under thermal and mechanical loads [36]. This method has also been used to study the thermal buckling on different shaped plates with different boundary conditions [21] as well as the thermomechanical flow of friction stir welding process, [46,49]. EFG can be used also to solve classical thermoelastic problems [10,50], such as hollow cylinder and infinite plate with a circular hole which are commonly used as benchmark problems. In [10], a combination between EFG and the improved moving least-squares approximation is proposed where the essential boundary conditions are imposed by the penalty method. Likewise EFG has been used to simulate the thermal fracture in functionally graded materials [13]. This method has also been used to analyze thermal–mechanical coupling of the orthotropic structures, [52].

The radial point interpolation method (RPIM) has been used in order to analyze thermoelastic problems with moving concentrated heat sources [23] where the Kronecker delta property is satisfied by its shape function. This method is also suitable to simulate thermomechanical crack growth, [34]. Several thermal and mechanical material properties have been identified simultaneously by using RPIM, [6]. Since this method requires background cells for numerical integration, efforts have been made to improve it such as the use of the Cartesian transformation method (CTM) where basically numerical integration is done without using background cells. In this sense, RPIM can be considered a truly meshfree method.

Another commonly used method is the local Petrov–Galerkin method that has been used to analyze thermomechanical shock fracture and heat conduction with residual stress due to welding in [31,32], respectively. Direct meshless local Petrov–Galerkin (DMLPG) is used as a way to solve the coupled thermoelasticity problem in [19]. This method is based on the weak solution of the governing equation, and all those methods have been found to be more efficient than FEM as we expected. Finally, the particle finite element method (PFEM) has been introduced in [39] to solve thermomechanical problems involving large strains, multiple contacts, rotations and large boundary surface changes and it was later used in the modeling of chip formation and metal cutting problems [40,41]. Besides good precision and stability, weak methods naturally satisfy Neumann-type boundary conditions. Moreover, these methods are computationally expensive due to the use of mandatory background meshes; therefore, strong form/truly meshfree methods as simpler alternatives are attractive.

With regard to the strong form methods, smoothed particle hydrodynamics (SPH) proposed by Lucy in [28] and Monaghan in [14] was the starting point of meshless methods. Nowadays, this method can be used to analyze a brake including thermomechanical coupling in [2], modeling of metal forging in [5] and large deformation problems in [1]. In [8], a numerical comparison between SPH and FEM in thermomechanical coupled problems has been made. Although the same numerical results were obtained with both methods, SPH overcomes the limitations of FEM as it was expected.

In the scientific literature, there are some works that use local radial basis function collocation method (LRBFCM) as a way to solve thermomechanical problems such as hot rolling simulation [15–18,43], linear thermoelasticity in two dimensions [29], bending analyses of quasicrystal plates [3], analysis of transient coupled thermoelasticity [30] and simulation of thermal field in mass concrete structures with cooling pipes [20].

Meshless local strong form method (MLSM) has been used in order to solve linear elastic problems under fretting contact conditions [25], a comparison between commercial software, weak and strong form methods has been made. This comparison shows that MLSM provides an accurate result with a significantly lower number of nodes. This method can also be used to solve the Cauchy–Navier equation [44]. This study reveals that MSLM can handle computations in com-

plex domains which is important in solving more complex real engineering problems. Other strong form methods that have been applied to elasticity problems include the finite point method [35] and the meshless finite difference method [22].

The finite pointset method is a meshfree method proposed by Kuhnert in [26]. This is a Lagrangian-type strong form method that has been used for modeling flows [48], for PDEs on evolving surfaces [45], heat transfer with moving heat sources in welding [37], fluid flow coupled with heat transfer considering phase changes [38] and recently, for solving static linear elasticity problems [42], among others. In fact, this is an efficient and versatile truly meshless method that is extended in this work and presented for the first time in a fully coupled form to numerically solve static linear thermoelastic problems.

The structure of the paper is as follows: Sect. 2 introduces the governing partial differential equations of static linear thermoelasticity, Sect. 3 shortly describes the main ideas behind the taken meshfree approach and a new fully coupled FPM discretization in detail for the involved PDEs is worked out. The corresponding numerical results and some comparisons with respect to analytical solutions are discussed in Sect. 4 followed by some conclusions and possible future work in last section.

2 Governing equations

The thermoelastic behavior in an isotropic and homogeneous conducting solid can be described once the temperature, stress and displacement fields are computed. For the study considered in this work, the displacement field obeys the Navier–Cauchy equations coupled with the stationary heat equation which can be written as:

$$(\lambda+\mu)\nabla(\nabla\cdot\mathbf{u})+\mu\nabla^2\mathbf{u}-\nabla(\beta(T-T_{\text{ref}}))=0 \tag{1}$$

$$\nabla(k\nabla T)=0 \tag{2}$$

For a two-dimensional problem, these equations could be expressed as follows:

$$(\lambda+\mu)\frac{\partial}{\partial x}\left(\frac{\partial u}{\partial x}+\frac{\partial v}{\partial y}\right)+\mu\left(\frac{\partial^2 u}{\partial x^2}+\frac{\partial^2 u}{\partial y^2}\right)-\frac{\partial(\beta(T-T_{\text{ref}}))}{\partial x}=0 \tag{3}$$

$$(\lambda+\mu)\frac{\partial}{\partial y}\left(\frac{\partial u}{\partial x}+\frac{\partial v}{\partial y}\right)+\mu\left(\frac{\partial^2 v}{\partial x^2}+\frac{\partial^2 v}{\partial y^2}\right)-\frac{\partial(\beta(T-T_{\text{ref}}))}{\partial y}=0 \tag{4}$$

$$\frac{\partial}{\partial x}\left(k\frac{\partial T}{\partial x}\right)+\frac{\partial}{\partial y}\left(k\frac{\partial T}{\partial y}\right)=0 \tag{5}$$

where λ and μ denote the Lamé coefficients and k is the thermal conductivity. The coefficient β is given by $\beta=(3\lambda+2\mu)\gamma$, where γ denotes the linear coefficient of thermal expansion.

The types of boundary conditions considered in this work are mainly essential or Dirichlet conditions which represent some prescribed displacement, denoted as $\mathbf{u}=\mathbf{u}_0$ and some prescribed temperature $T=T_0$ on some portions of the defined boundary. In a similar manner, traction or natural boundary conditions, denoted as $\sigma\mathbf{n}=\mathbf{t}_0$, which represent some prescribed surface traction in a specified boundary region as well as some temperature gradient or heat flux denoted by $(k(x)\nabla T)\cdot\mathbf{n}=q_0$, prescribed on a given boundary. σ denotes the stress tensor which for a linear thermoelastic problem could be expressed as

$$\sigma=[\lambda\text{tr}(\varepsilon)-\beta(T-T_{\text{ref}})]I+2\mu\varepsilon,\quad \varepsilon=\frac{\nabla\mathbf{u}+(\nabla\mathbf{u})^t}{2} \tag{6}$$

where I and ε are the identity and strain tensors, respectively. $\mathbf{t}_0=(t_{01},t_{02})^t$ is the traction vector and $\mathbf{n}=(n_1,n_2)^t$ denotes the unit normal vector. If a thermoelastic problem with essential boundary conditions is considered, the boundary conditions can be written as follows

$$t_{01}=\mu n_2\frac{\partial u}{\partial y}+\lambda n_1\frac{\partial v}{\partial y}+(2\mu+\lambda)n_1\frac{\partial u}{\partial x}+\mu n_2\frac{\partial v}{\partial x}-\beta(T-T_{\text{ref}})n_1 \tag{7}$$

$$t_{02}=\mu n_1\frac{\partial u}{\partial y}+(2\mu+\lambda)n_2\frac{\partial v}{\partial y}+\lambda n_2\frac{\partial u}{\partial x}+\mu n_1\frac{\partial v}{\partial x}-\beta(T-T_{\text{ref}})n_2 \tag{8}$$

$$q_0=n_1k(x)\frac{\partial T}{\partial x}+n_2k(x)\frac{\partial T}{\partial y} \tag{9}$$

With all these definitions, it is possible to model the static linear thermoelastic problem correctly.

3 FPM discretization for general elliptic partial differential equations

In this section, a short description on FPM discretization for elliptic partial differential equations in a general form is described which has been already presented in [42]. Consider the numerical solution of an elliptic PDE with the form:

$$A_1\psi+\mathbf{B}\cdot\nabla\psi+C_1\Delta\psi-F=0 \tag{10}$$

with prescribed boundary conditions, where A_i, $\mathbf{B}$, C_i, F and φ are known. Thus, the corresponding FPM discretization under this setting and considering the general case with Robin boundary conditions is shortly sketched.

Consider the Taylor expansion of $\psi(\mathbf{x}_i)$ around a point $\mathbf{x} \in \Gamma_r$

$$\psi(\mathbf{x}_i) = \psi(\mathbf{x}) + \sum_{k=1}^{3} \frac{\partial \psi}{\partial x_k}(x_{k,i} - x_k) + \frac{1}{2}\sum_{j,k=1}^{3} \frac{\partial^2 \psi}{\partial x_k \partial x_j}(x_{k,i} - x_k)(x_{j,i} - x_j) + e_{1,i}$$

for $i = 1, \ldots, m$, where $e_{1,i}$ denotes the truncation error of the Taylor series expansion and m is the number of points inside the neighborhood of $\mathbf{x}$ which is defined through a Gaussian weight function w whose form is given by

$$w(\mathbf{x} - \mathbf{x}_i) = \begin{cases} e^{-\alpha \|\mathbf{x}-\mathbf{x}_i\|^2/h^2}, & \text{if } \frac{\|\mathbf{x}-\mathbf{x}_i\|}{h} \leq 1 \\ 0 & \text{else} \end{cases} \tag{11}$$

where h defines the interaction length between nodes and it is called the smoothing length.

A linear system of $m + 2$ equations is obtained when the m Taylor series expansions for $\psi(\mathbf{x}_i)$ are taken together with the elliptic partial differential equation and the corresponding boundary conditions. This linear system can be written in matrix form as

$$\mathbf{e} = M\mathbf{a}_\psi - \mathbf{b} \tag{12}$$

where

$$M = \begin{pmatrix} 1 & h_{1,1} & h_{2,1} & h_{3,1} & \frac{1}{2}h_{1,1}^2 & h_{1,1}h_{2,1} & h_{1,1}h_{3,1} & \frac{1}{2}h_{2,1}^2 & h_{2,1}h_{3,1} & \frac{1}{2}h_{3,1}^2 \\ 1 & h_{1,2} & h_{2,2} & h_{3,2} & \frac{1}{2}h_{1,2}^2 & h_{1,2}h_{2,2} & h_{1,2}h_{3,2} & \frac{1}{2}h_{2,2}^2 & h_{2,2}h_{3,2} & \frac{1}{2}h_{3,2}^2 \\ \vdots & \vdots & \vdots & \vdots & \vdots & \vdots & & & & \\ 1 & h_{1,m} & h_{2,m} & h_{3,m} & \frac{1}{2}h_{1,m}^2 & h_{1,m}h_{2,m} & h_{1,m}h_{3,m} & \frac{1}{2}h_{2,m}^2 & h_{2,m}h_{3,m} & \frac{1}{2}h_{3,m}^2 \\ A_1 & B_1 & B_2 & B_3 & C_1 & 0 & 0 & C_1 & 0 & C_1 \\ A_2 & C_2 n_1 & C_2 n_2 & C_2 n_3 & 0 & 0 & 0 & 0 & 0 & 0 \end{pmatrix} \tag{13}$$

with $h_{1,j} = (x_{1,j} - x_1)$, $h_{2,j} = (x_{2,j} - x_2)$ and $h_{3,j} = (x_{3,j} - x_3)$,

$$\mathbf{a}_\psi = \left(\psi, \frac{\partial \psi}{\partial x_1}, \frac{\partial \psi}{\partial x_2}, \frac{\partial \psi}{\partial x_3}, \frac{\partial^2 \psi}{\partial x_1{}^2}, \frac{\partial^2 \psi}{\partial x_1 \partial x_2}, \frac{\partial^2 \psi}{\partial x_1 \partial x_3}, \frac{\partial^2 \psi}{\partial x_2{}^2}, \frac{\partial^2 \psi}{\partial x_2 \partial x_3}, \frac{\partial^2 \psi}{\partial x_3{}^2}\right)^t \tag{14}$$

$$\mathbf{b} = (\psi_1, \psi_2, \ldots, \psi_m, F, \varphi)^t \tag{15}$$

$$\mathbf{e} = (e_1, e_2, \ldots, e_m, e_{m+1}, e_{m+2})^t \tag{16}$$

and $\mathbf{n} = (n_1, n_2, n_3)^t$ denotes the unitary normal vector to the boundary. The unknown vector $\mathbf{a}_\psi$ is obtained trough the weighted least-squares method as

$$\mathbf{a}_\psi = (M^t W M)^{-1}(M^t W)\mathbf{b}, \tag{17}$$

where W is

$$W = \begin{bmatrix} w(\mathbf{x} - \mathbf{x}_1) & 0 & \cdots & 0 & 0 & 0 \\ 0 & w(\mathbf{x} - \mathbf{x}_2) & \cdots & 0 & 0 & 0 \\ \vdots & \vdots & \ddots & \vdots & \vdots & \vdots \\ 0 & 0 & \cdots & w(\mathbf{x} - \mathbf{x}_n) & 0 & 0 \\ 0 & 0 & \cdots & 0 & 1 & 0 \\ 0 & 0 & \cdots & 0 & 0 & 1 \end{bmatrix} \tag{18}$$

Depending on where the point lies, that is, if $\mathbf{x}_i \in \Gamma_d$, $\mathbf{x}_i \in \Gamma_n$ or $\mathbf{x}_i \in \Omega$, some rows in M must be carefully replaced or deleted. Details can be found in [42].

Considering the following solution

$$\mathbf{a}_\psi = Q(M^t W)\mathbf{b}, \tag{19}$$

and taking $\mathbf{q} = (q_{1,1}, q_{1,2}, \ldots, q_{1,10})$ as the first row of Q, the following linear system of equations arises

$$\psi_j - \sum_{i=1}^{m_j} w_{j_i} \Big(q_{1,1} + q_{1,2}h_{1,i} + q_{1,3}h_{2,i} + q_{1,4}h_{3,i} + q_{1,5}\frac{h_{1,i}^2}{2} + q_{1,6}h_{1,i}h_{2,i} + q_{1,7}h_{1,i}h_{3,i} + q_{1,8}\frac{h_{2,i}^2}{2} + q_{1,9}h_{2,i}h_{3,i} + q_{1,10}\frac{h_{3,i}^2}{2}\Big)\psi_{j_i}$$

$$= (q_{1,1}A_1 + q_{1,2}B_1 + q_{1,3}B_2 + q_{1,4}B_3 + q_{1,5}C_1 + q_{1,8}C_1 + q_{1,10}C_1)F + (q_{1,1}A_2 q_{1,2}C_2 n_x + q_{1,3}C_2 n_y + q_{1,4}C_2 n_z)\varphi \quad (20)$$

where ψ_j denotes the unknown function values at point j and m_j the number of jth-neighboring nodes inside its neighborhood defined by the weight function. It explicitly couples each point with its neighbor nodes which leads the coupling between inner and boundary points. Since Eq. (20) is valid for $j = 1, 2, \ldots, N$, this can be arranged in a global sparse system of linear equations $K\tilde{\Psi} = \mathbf{f}$ which can be solved by iterative methods.

3.1 FPM discretization for static linear thermoelasticity equations

The procedure to obtain the global system of equations described in the last section can be extended for the two-dimensional static linear thermoelasticity equations as it is shown along this section. Consider the Taylor expansions for the two approximating solution functions of the coupled system of PDE equations,

$$u_i = u + \sum_{k=1}^{3} \frac{\partial u}{\partial x_k}(x_{k,i} - x_k) + \frac{1}{2}\sum_{j,k=1}^{3} \frac{\partial^2 u}{\partial x_k \partial x_j}(x_{k,i} - x_k)(x_{j,i} - x_j) + e_{1,i}$$

$$v_i = v + \sum_{k=1}^{3} \frac{\partial v}{\partial x_k}(x_{k,i} - x_k) + \frac{1}{2}\sum_{j,k=1}^{3} \frac{\partial^2 v}{\partial x_k \partial x_j}(x_{k,i} - x_k)(x_{j,i} - x_j) + e_{2,i}$$

$$T_i = T + \sum_{k=1}^{3} \frac{\partial T}{\partial x_k}(x_{k,i} - x_k) + \frac{1}{2}\sum_{j,k=1}^{3} \frac{\partial^2 T}{\partial x_k \partial x_j}(x_{k,i} - x_k)(x_{j,i} - x_j) + e_{3,i}$$

where $e_{1,i}$, $e_{2,i}$ and $e_{3,i}$ denote the errors of the Taylor series expansion. As in the previous section, together with these equations, (3), (4) and (5) with the corresponding boundary conditions should be also considered. $\mathbf{u} = \mathbf{u_0} = (u_0, v_0)$ and $T = T_0$ in case of Dirichlet boundary conditions for displacement and temperature, or Eqs. (7), (8) and (9) in case of Neumann boundary conditions which is the most involved case explained next. If $\mathbf{x} \in \Gamma_n$, a linear system of $m + 6$ equations is obtained which in terms of the truncation error can be written as,

$$\mathbf{e} = \tilde{M}\mathbf{a} - \mathbf{b}$$

where

$$\tilde{M} = \begin{pmatrix} M & \mathbf{0} & \mathbf{0} \\ \mathbf{0} & M & \mathbf{0} \\ \mathbf{0} & \mathbf{0} & M \\ J_1 & J_2 & J_3 \end{pmatrix}$$

and

$$\mathbf{e} = (e_{1,1}, \ldots, e_{1,m}, e_{2,1}, \ldots, e_{2,m}, e_{3,1}, \ldots, e_{3,m}, 0, 0, 0, 0, 0, 0)^t$$

$$\mathbf{b} = (u_1, \ldots, u_m, v_1, \ldots, v_m, T_1, \ldots, T_m, 0, 0, 0, t_{0,1} - \beta n_1 T_{\text{ref}}, t_{0,2} - \beta n_2 T_{\text{ref}}, q_0)^t$$

$$\mathbf{a} = (\mathbf{a}_u, \mathbf{a}_v, \mathbf{a}_T)^t$$

$$\mathbf{a}_u = \left(u, \frac{\partial u}{\partial x_1}, \frac{\partial u}{\partial x_2}, \frac{\partial^2 u}{\partial x_1^2}, \frac{\partial^2 u}{\partial x_1 \partial x_2}, \frac{\partial^2 u}{\partial x_2^2}\right)^t$$

$$\mathbf{a}_v = \left(v, \frac{\partial v}{\partial x_1}, \frac{\partial v}{\partial x_2}, \frac{\partial^2 v}{\partial x_1^2}, \frac{\partial^2 v}{\partial x_1 \partial x_2}, \frac{\partial^2 v}{\partial x_2^2}\right)^t$$

$$\mathbf{a}_T = \left(T, \frac{\partial T}{\partial x_1}, \frac{\partial T}{\partial x_2}, \frac{\partial^2 T}{\partial x_1^2}, \frac{\partial^2 T}{\partial x_1 \partial x_2}, \frac{\partial^2 T}{\partial x_2^2}\right)^t$$

M is of the same form as in the original FPM discretization for elliptic PDEs. Moreover, matrices J_1, J_2 and J_3 are defined as follows,

$$J_1 = \begin{pmatrix} 0 & 0 & 0 & 2\mu + \lambda & 0 & \mu \\ 0 & 0 & 0 & 0 & \lambda + \mu & 0 \\ 0 & 0 & 0 & 0 & 0 & 0 \\ 0 & (2\mu + \lambda)n_1 & \mu n_2 & 0 & 0 & \mu \\ 0 & \lambda n_2 & \mu n_1 & 0 & 0 & 0 \\ 0 & 0 & 0 & 0 & 0 & 0 \end{pmatrix},$$

$$J_2 = \begin{pmatrix} 0 & 0 & 0 & 0 & \lambda + \mu & 0 \\ 0 & 0 & 0 & \mu & 0 & 2\mu + \lambda \\ 0 & 0 & 0 & 0 & 0 & 0 \\ 0 & \mu n_2 & \lambda n_1 & 0 & 0 & 0 \\ 0 & \mu n_1 & (2\mu + \lambda)n_2 & 0 & 0 & 0 \\ 0 & 0 & 0 & 0 & 0 & 0 \end{pmatrix}$$

and

$$J_3 = \begin{pmatrix} 0 & -\beta & 0 & 0 & 0 & 0 \\ 0 & 0 & -\beta & 0 & 0 & 0 \\ 0 & 0 & 0 & k & 0 & k \\ -\beta n_1 & 0 & 0 & 0 & 0 & 0 \\ -\beta n_2 & 0 & 0 & 0 & 0 & 0 \\ 0 & n_1 & n_2 & 0 & 0 & 0 \end{pmatrix}$$

Following the procedure in the previous section, the corresponding solution for the linear system can be written as

$$\mathbf{a} = (\tilde{M}^t W \tilde{M})^{-1} (\tilde{M}^t W)\mathbf{b} \tag{21}$$

Therefore, for the computation of the displacements and temperature fields, only the first, seventh and thirteenth components in **a** are really needed. Consequently if

$$\mathbf{q}_i = (q_{i,1}, q_{i,2}, \ldots, q_{i,18})^t$$

denotes the ith row in $(\tilde{M}^t W \tilde{M})^{-1}$, Eq. (21) can be slightly worked out and the following linear system arises for the elements of the displacement vector **u** and T,

$$\begin{aligned}
u_j - \sum_{i=1}^{m_j} w \Big[& \Big(q_{k,1} + h_{1,i} q_{k,2} + h_{2,i} q_{k,3} \\
& + \frac{1}{2} h_{1,i}^2 q_{k,4} + h_{1,i} h_{2,i} q_{k,5} + \frac{1}{2} h_{2,i}^2 q_{k,6}\Big) u_i \\
& + \Big(q_{k,7} + h_{1,i} q_{k,8} + h_{2,i} q_{k,9} \\
& + \frac{1}{2} h_{1,i}^2 q_{k,10} + h_{1,i} h_{2,i} q_{k,11} + \frac{1}{2} h_{2,i}^2 q_{k,12}\Big) v_i \\
& + \Big(q_{k,13} + h_{1,i} q_{k,14} + h_{2,i} q_{k,15} \\
& + \frac{1}{2} h_{1,i}^2 q_{k,16} + h_{1,i} h_{2,i} q_{k,17} + \frac{1}{2} h_{2,i}^2 q_{k,18}\Big) T_i \Big] \\
= & [(2\mu + \lambda) n_1 q_{k,2} + \mu n_2 (q_{k,3} + q_{k,8}) \\
& + \lambda n_1 q_{k,9} - \beta n_1 q_{k,13}](t_{0,1} - \beta n_1 T_{\text{ref}}) \\
& + [\lambda n_2 q_{k,2} + \mu n_1 (q_{k,3} + q_{k,8}) \\
& + (2\mu + \lambda) n_2 q_{k,9} - \beta n_2 q_{k,13}](t_{0,2} - \beta n_1 T_{\text{ref}}) \\
& + [n_1 q_{k,14} + n_2 q_{k,15}] q_0
\end{aligned} \tag{22}$$

for the component u. A similar expression can be obtained for the component v and T on the jth point. This is valid for all $u_j, v_j, T_j \in \Gamma_n$ where $k = 1, 7, 13$. Furthermore, an homogeneous linear system in (22) is obtained for internal domain points where in such case the last three rows in $\tilde{M}$ and elements in **b** must be deleted. Finally, using this last formulation for the displacement and temperature fields, a coupled sparse linear system, $K\tilde{\Psi} = \mathbf{f}$, can be obtained which is numerically solved by iterative methods. Once these displacements and temperatures are computed, the stress can be obtained locally from the moving least-squares solution (21) with a updated vector **b** and the corresponding deformation values. Thus, the numerical solution of another sparse system for the computation of these quantities is not necessary.

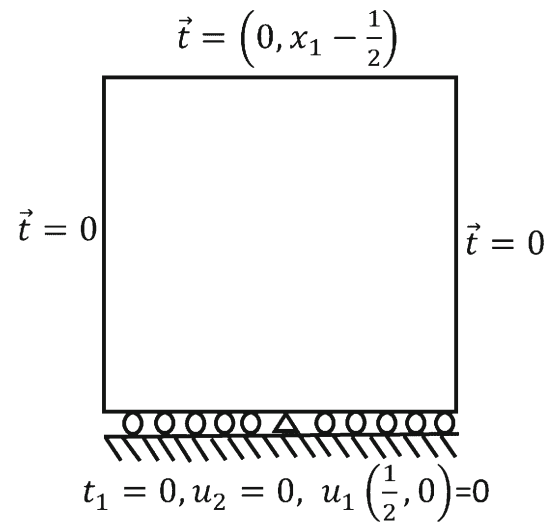

Fig. 1 Problem configuration

4 Numerical examples

In order to test the numerical performance of the proposed FPM coupled discretization, four examples are presented in this section. These examples have been taken from [29] and [51], and they were computed on a AMD A10-7400P CPU 2.5GHz processor running Windows 10 Home operating system with 12 GB of RAM. The physical difficulty of the presented examples is gradually increasing.

In order to measure the approximating solution error regarding the obtained displacements, von Mises stresses and the corresponding temperatures, the following relative error norms are used,

$$e_\infty(\mathbf{u}) = \frac{\max_{x \in X}\{\max\{|u(\mathbf{x}) - \hat{u}(\mathbf{x})|, |v(\mathbf{x}) - \hat{v}(\mathbf{x})|\}\}}{\max_{x \in X}\{|u(\mathbf{x})|, |v(\mathbf{x})|\}} \tag{23}$$

$$e_\infty(\sigma_v) = \frac{\max_{x \in X} |\sigma_v(\mathbf{x}) - \hat{\sigma}_v(\mathbf{x})|}{\max_{x \in X} |\sigma_v(\mathbf{x})|} \tag{24}$$

$$e_\infty(T) = \frac{\max_{x \in X} |T(\mathbf{x}) - \hat{T}(\mathbf{x})|}{\max_{x \in X} |T(\mathbf{x})|} \tag{25}$$

$$e_2(\mathbf{u}) = \frac{\left\|\mathbf{u}(\mathbf{x}) - \hat{\mathbf{u}}(\mathbf{x})\right\|}{\left\|\hat{\mathbf{u}}(\mathbf{x})\right\|} \tag{26}$$

$$e_2(\sigma_v) = \frac{|\sigma_v(\mathbf{x}) - \hat{\sigma}_v(\mathbf{x})|}{|\hat{\sigma}_v(\mathbf{x})|} \tag{27}$$

$$e_2(T) = \frac{|T(\mathbf{x}) - \hat{T}(\mathbf{x})|}{|\hat{T}(\mathbf{x})|} \tag{28}$$

where X denotes the set of nodes.

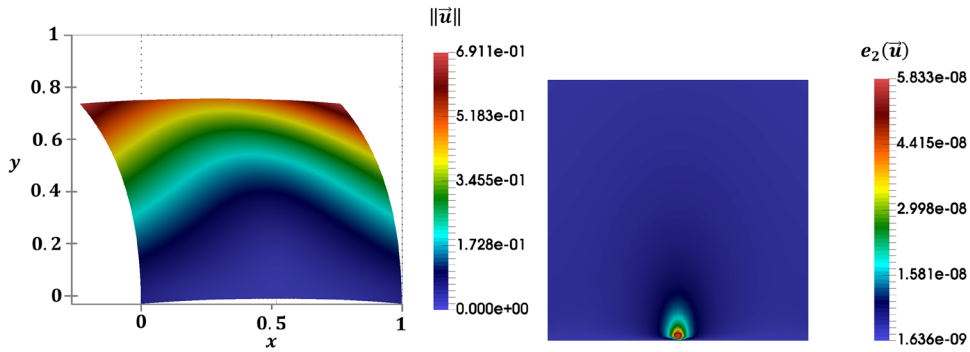

Fig. 2 *Left:* FPM solution error with respect to the exact solution. *Right:* error comparison. n is the number of support nodes and $\hat{\sigma}$ is a Gaussian weight shape parameter

4.1 Bending of an isothermal square

The first benchmark problem is geometrically described in Fig. 1 together with the corresponding boundary conditions. In this case a linearly increasing force is applied on the top boundary in order to deform the isothermal square. The corresponding analytical solution for the displacements reads,

$$u = \frac{-\lambda}{8\mu(\lambda+\mu)}\left(x_1 - \frac{1}{2}\right)^2 - \frac{(\lambda+2\mu)}{8\mu(\lambda+\mu)}x_2^2 \tag{29}$$

$$v = \frac{(\lambda+2\mu)}{4\mu(\lambda+\mu)}\left(x_1 - \frac{1}{2}\right)x_2 \tag{30}$$

The reported numerical results in this case were obtained considering $\lambda = 0.4$, $\mu = 0.4$, $\gamma = 1$ using a discretization of 1681 points with a mean spacing of 0.025 m, $\alpha = 16.25$ and a smoothing length of 0.075 m.

Figure 2 shows the magnitude of the obtained displacement on the deformed square and the corresponding error with respect to the analytical solution. The displacement has been scaled by a factor of 0.5 for visualization purposes. As it can be observed, the highest value in the numerical error is of the order of 10^{-8} which is valid for several configurations regarding the number of points and their distribution. This shows an excellent numerical behavior of FPM in this case.

4.2 Thermal expansion of a square

The second tested problem consists of a thermal expansion of a square with a temperature profile defined by $T(x_1, x_2) = \sin(2\pi x_1)$. The geometry and the boundary conditions are depicted in Fig. 3. The exact analytical solution corresponding to the displacements reads,

$$u = -\frac{\gamma(3\lambda+2\mu)[\cos(2\pi x_1) - 1]}{2\pi(\lambda+2\mu)} \tag{31}$$

$$v = 0 \tag{32}$$

The reported numerical results in this case were obtained considering $\lambda = 0.4$, $\mu = 0.4$, $\gamma = 1$ using a discretization of 1681 points with a mean spacing of 0.025 m, $\alpha = 16.25$ and a smoothing length of 0.075 m.

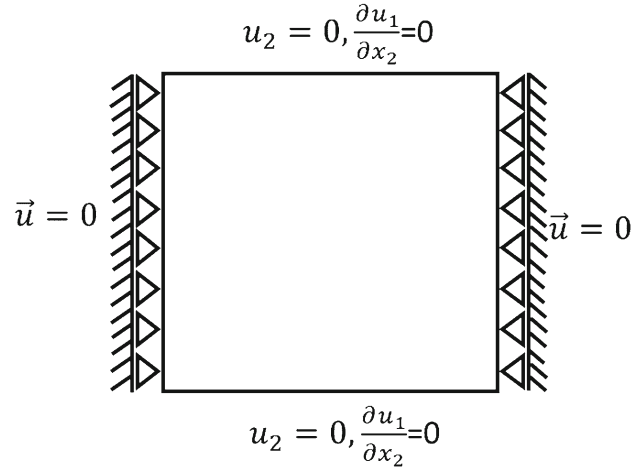

Fig. 3 Problem configuration

Figure 4 shows the magnitude of the obtained displacement on the thermal expanded square and the corresponding error with respect to the analytical solution. As it can be observed, the maximum computed error is of the order of 10^{-3}. The value of α in the shape function is used to emphasize the effect of the closest neighbors, such that neighbor particles with the smallest distance to the central node have the highest weight. Thus, it is dependent on the nature of the case being analyzed. For example, for solving the incompressible Navier–Stokes equations values around 6 have shown good results [47], for coupled fluid flow and heat transfer values around 5 were selected [38], and for solid mechanics problems, values around 12 were chosen [42]. Therefore, the influence of α on the numerical accuracy for this example is described in Fig. 5 in order to select a suitable value for thermoelasticity problems. This figure suggests that a suitable value for α should be higher than 15 since from this value, the error no longer significantly decreases with the increase of α, and therefore, for the numerical examples presented in this work a value of 16.25 was chosen. In a similar manner, the number of neighboring points has been chosen

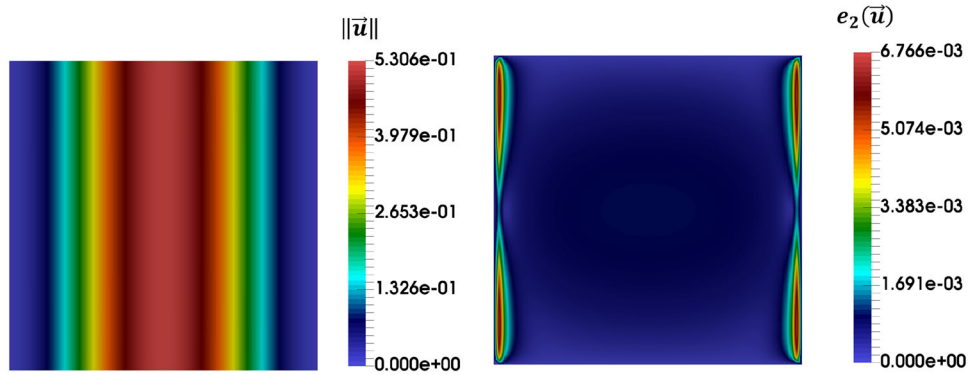

Fig. 4 *Left:* Displacement magnitude. *Right:* Pointwise displacement relative error

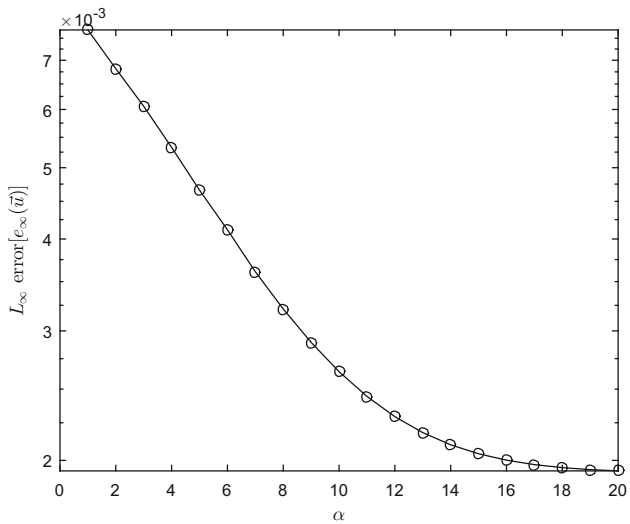

Fig. 5 Displacement relative error in L_∞-norm with respect to alpha

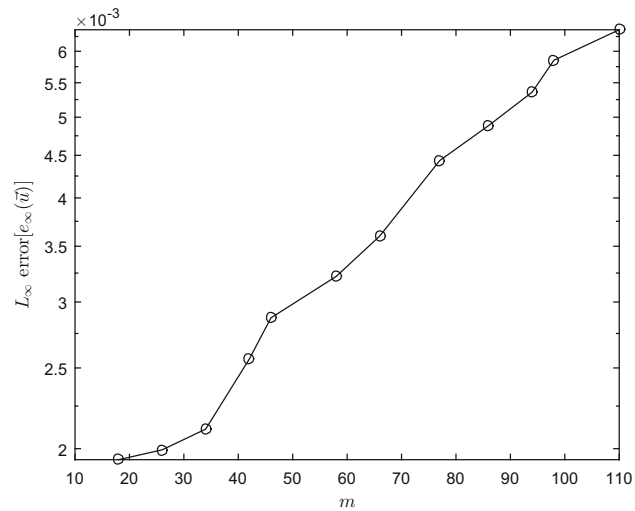

Fig. 6 Displacement relative error in L_∞-norm with respect to number of neighboring points

according to the reported error in Fig. 6, where the displacement relative error with respect to the number of neighboring points increases as the number of points in the shape function support also increases. Stability dispersion is shown in Fig. 7 with respect to several degrees of increment on the perturbation parameter δ which defines the distortion of the uniform distribution, see [44] for more details. It shows that this meshfree formulation is independent of the uniformity of the nodes discretizing the domain since, for a uniformly distributed distribution and a very distorted one, this proposal is able to get results with the same level of accuracy. For completeness, Fig. 8 shows the displacement error behavior with respect to the total number of points and Fig. 9 reports the FPM spent total time when solving the problem with respect to the number of discretization nodes. They indicate a good convergence behavior and an efficient computational strategy with respect to the increasing discretization points.

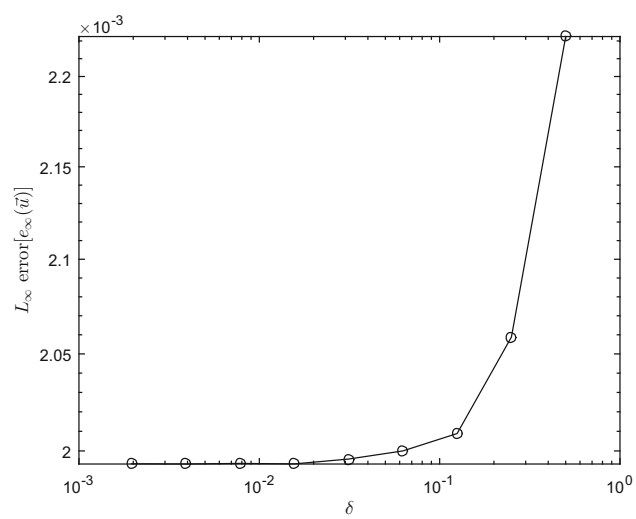

Fig. 7 Displacement relative error in L_∞-norm with respect to points dispersion

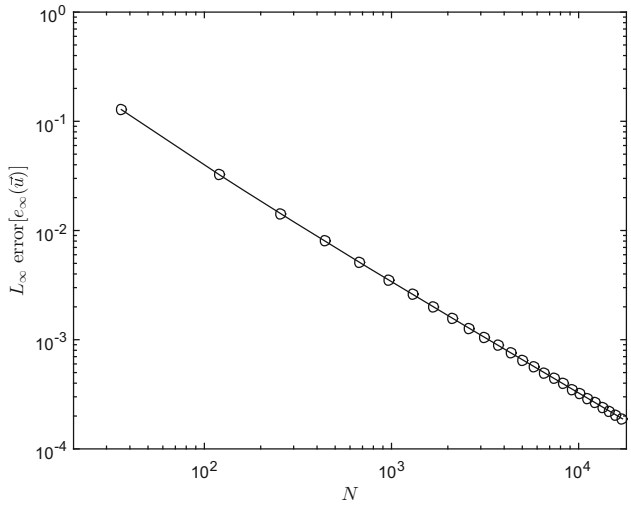

Fig. 8 Displacement relative error in L_∞-norm with respect to total number of points

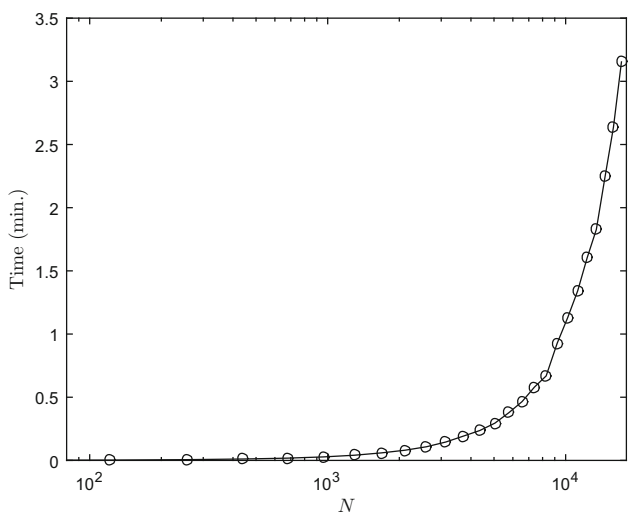

Fig. 9 Total computation time with respect to total number of points

4.3 Ring plate

The third benchmark problem consists in the simulation of the thermoelastic state of a ring. The corresponding problem configuration and geometrical description are shown in Fig. 10.

The analytical solution for the involved variables is defined in polar coordinates as follows [51]:

– The analytical expression for temperature,

$$T(r) = 1 - \frac{\ln(r)}{\ln(2)} \tag{33}$$

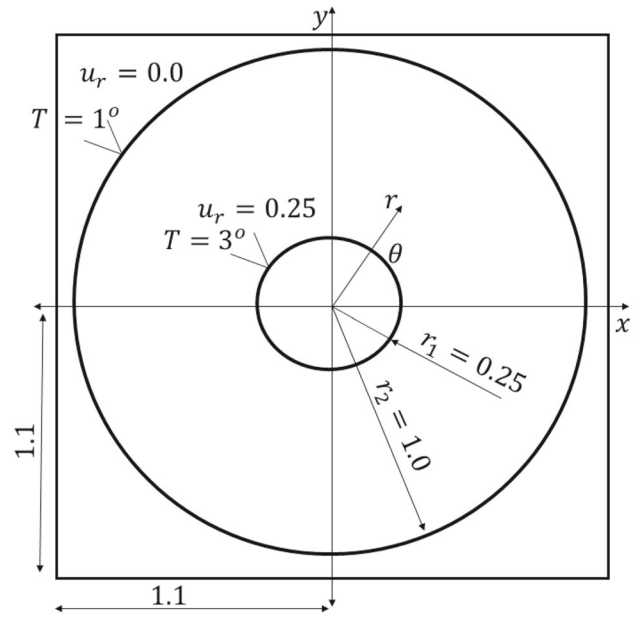

Fig. 10 Problem configuration

– The displacement of the ring,

$$u_r(r) = -\frac{r\ln(r)}{2\ln(2)} \tag{34}$$

$$u_\theta(r) = 0 \tag{35}$$

– The strain,

$$\varepsilon_r(r) = \frac{\partial u_r}{\partial r} = -\frac{\ln(r)+1}{2\ln(2)} \tag{36}$$

$$\varepsilon_\theta(r) = \frac{1}{r}\frac{\partial u_\theta}{\partial \theta} + \frac{u_r}{r} = -\frac{\ln(r)}{2\ln(2)}, \tag{37}$$

$$\varepsilon_{r\theta}(r) = \frac{1}{2}\left(\frac{1}{r}\frac{\partial u_r}{\partial \theta} + \frac{\partial u_\theta}{\partial r} - \frac{u_\theta}{r}\right) = 0 \tag{38}$$

– The plane stress,

$$\begin{aligned}\sigma_r(r) &= \frac{E}{1-\nu^2}[\varepsilon_r + \nu\varepsilon_\theta - (1+\nu)\gamma(T - T_{\text{ref}})] \\ &= \varepsilon_r(r) - T(r),\end{aligned} \tag{39}$$

$$\begin{aligned}\sigma_\theta(r) &= \frac{E}{1-\nu^2}[\varepsilon_\theta + \nu\varepsilon_r - (1+\nu)\gamma(T - T_{\text{ref}})] \\ &= \varepsilon_r(\theta) - T(r),\end{aligned} \tag{40}$$

$$\sigma_{r\theta}(r) = \frac{E}{1+\nu}\varepsilon_{r\theta} = 0 \tag{41}$$

The reported numerical results in this case were obtained considering $\lambda = 0$, $\mu = 0.5$, $\gamma = 1$ using a discretization of 2081 points with a mean spacing of 0.05 m, $\alpha = 16.25$ and a smoothing length of 0.15 m.

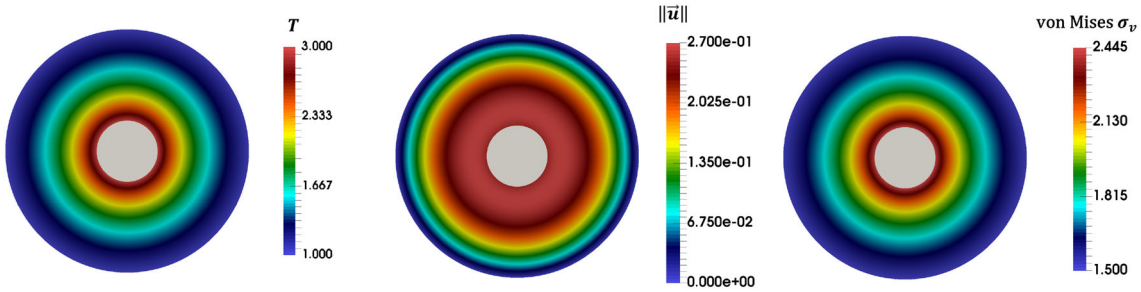

Fig. 11 *Left:* Temperature profile. *Middle:* Displacement magnitude. *Right:* von Mises stress profile

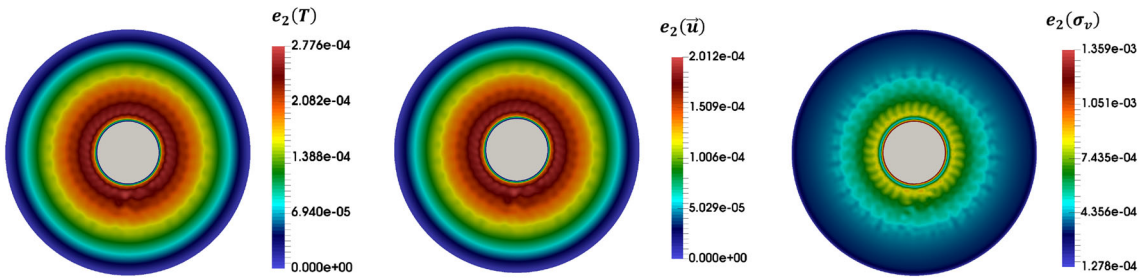

Fig. 12 *Left:* Temperature relative error. *Middle:* Displacement relative error. *Right:* von Mises stress relative error

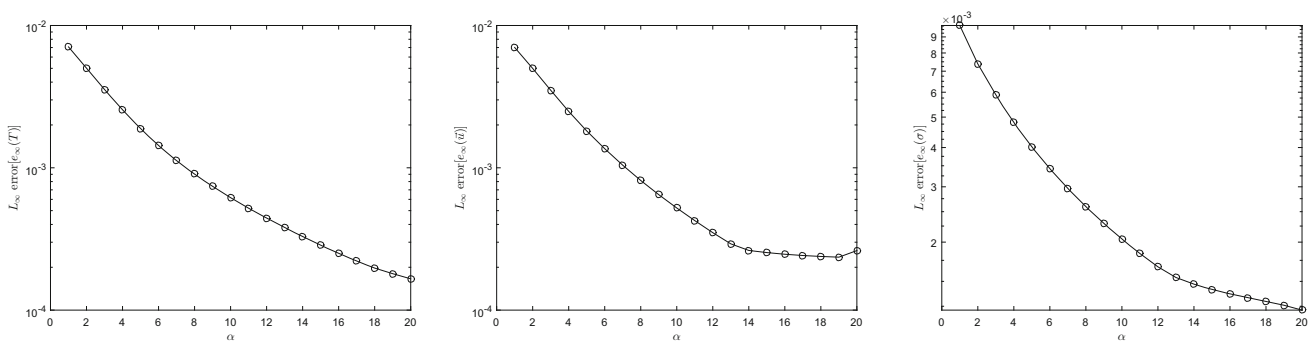

Fig. 13 Relative error in L_∞-norm with respect to alpha. *Left:* Temperature. *Middle:* Displacement. *Right:* von Mises stress

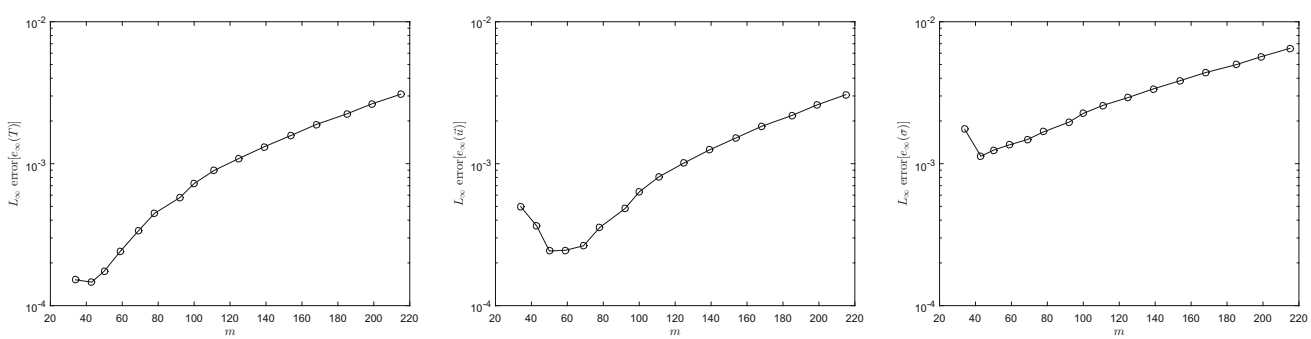

Fig. 14 Relative error in L_∞-norm with respect to number of neighboring points. *Left:* Temperature. *Middle:* Displacement. *Right:* von Mises stress

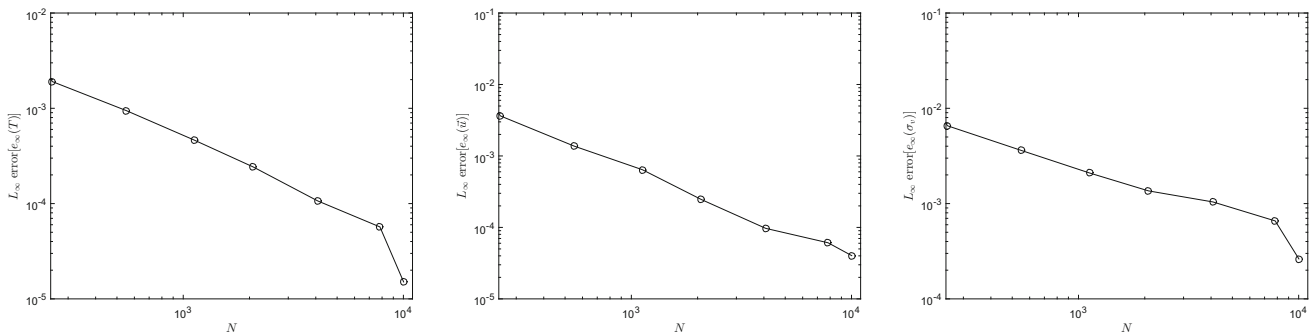

Fig. 15 Relative error in L_∞-norm with respect to total number of points. *Left:* Temperature. *Middle:* Displacement. *Right:* von Mises stress

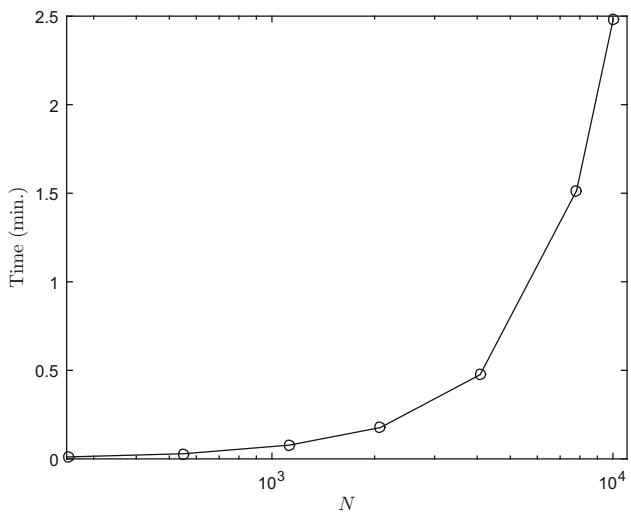

Fig. 16 Total computation time with respect to total number of points

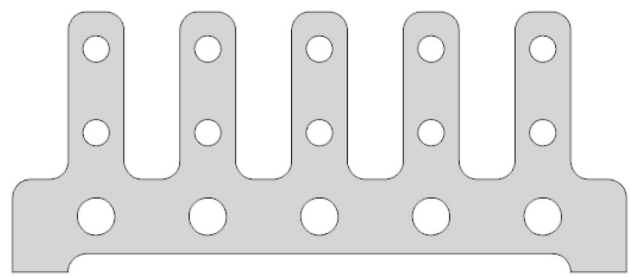

Fig. 17 Geometry of heat exchanging device

Figure 11 shows the obtained displacement, temperature and von Mises stress profiles computed with this FPM approach, and Fig. 12 shows the relative error of the obtained displacement, temperature and von Mises stress with respect to the analytical solution. As it can be observed the maximum computed error is of the order of 10^{-4} which shows an excellent match of the computed solution.

Figure 13 shows the error behavior with respect to α in the shape function for the three quantities. This one again suggests and confirms that a suitable value for α should be higher than 15. In a similar manner, the number of neighboring points has been chosen according to the reported error in Fig. 14, where the displacement, temperature and von Mises stress relative error with respect to the number of neighboring points increase as the number of points in the shape function support also increases. Finally, Fig. 15 shows the error behavior with respect to the total number of points and Fig. 16 reports the FPM spent total time when solving the problem with respect to the number of discretization nodes. As for the previous example, they indicate a good convergence behavior and an acceptable computational efficiency.

4.4 Heat exchanging device

The last and more realistic example is depicted in Fig. 17. The aim in this example is to compute the thermoelastic state in a complex geometry. In this example, a hot medium heats the device to 60° inside the boreholes. A surrounding medium establishes a temperature of 35° on the outside.

The reported numerical results in this case were obtained considering $\lambda = 6.05 \cdot 10^{10}$, $\mu = 2.59 \cdot 10^{10}$, $\gamma = 23 \cdot 10^{-6}$, $k = 237$ and $T_{\text{ref}} = 0$ using a discretization of 4091 points with a mean spacing of 0.3 m, $\alpha = 16.25$ and a smoothing length of 0.9 m.

The corresponding numerical results are reported in Fig. 18. The reached temperature profile distribution is shown at the top of the figure, the magnitude of the displacement and the corresponding deformation scaled by a factor of 50 (for visualization purposes) are shown at the middle of the picture and the von Mises stress is also reported at the bottom of this figure. This numerical example shows the generality of the method for dealing with distorted and complex domains. These results indicates the robustness and effectiveness of this coupled formulation for dealing with problems involving linear thermomechanical processes.

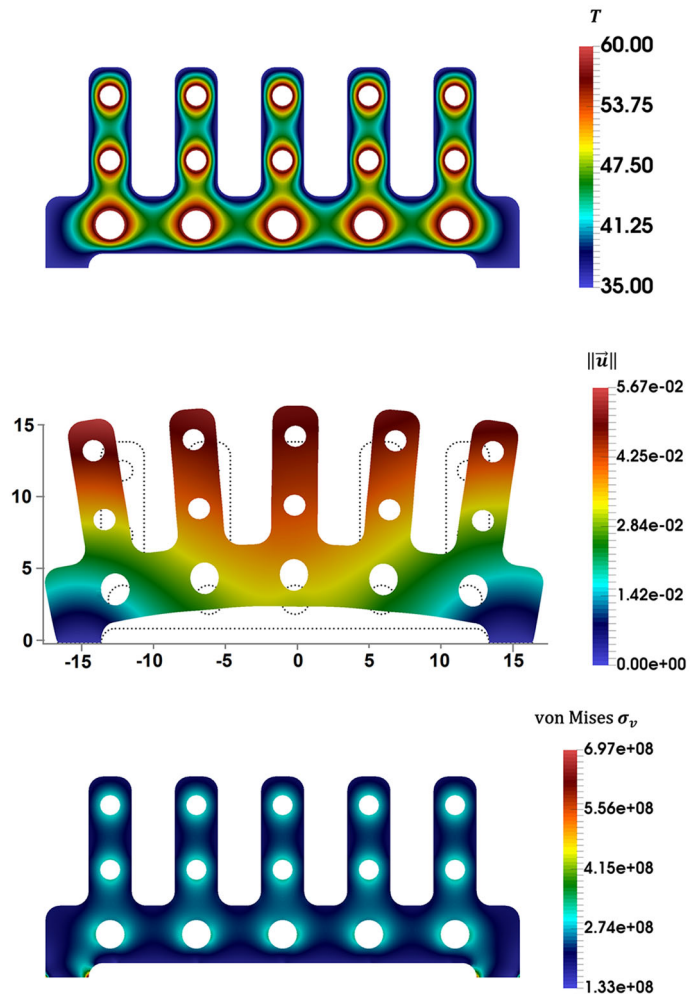

Fig. 18 *Top:* Temperature profile. *Middle:* Displacement magnitude. *Bottom:* von Mises stress profile

5 Conclusions

A fully coupled FPM mathematical derivation for two-dimensional static linear thermoelastic problems has been presented in detail and numerically implemented for the first time. Considering the numerical reported results, it can be said that FPM is a powerful and versatile strong form mesh-free approach for these kinds of solid mechanics problems. The identification of the involved parameters for an efficient FPM implementation has been done in a robust manner using the corresponding relative error analysis. The easy-to-handle boundary conditions in FPM are one featured that shall be stood out and this can be observed in the excellent matching with respect to the corresponding analytical solutions in the numerical examples. Although a fully coupled approach has been proposed in this paper, only one way coupling has been of interest in this work, i.e., the temperature dependence of the deformation is present; however, if a two-way coupling is considered this formulation could also work in an efficient manner with the correct form of the involved deformation tensor and this can be considered as an natural extension of this work in the near future. Furthermore, this approach is a promising numerical tool which could be coupled with mass transfer computations to achieve a fully coupled multi-physics formulation. As a future research, the extension to transient linear and nonlinear thermoelastic problems is of particular interest.

Declarations

Conflict of interest The authors declare that they have no conflict of interest.

References

1. Ba K, Gakwaya A (2018) Thermomechanical total Lagrangian SPH formulation for solid mechanics in large deformation problems. Comput Methods Appl Mech Eng 342:458–473
2. Baranowski P, Damaziak K, Malachowski J (2011) Analysis of a brake including thermomechanical coupling. In: Proceedings of the 19th international conference on computer methods in mechanics, pp 123–124

3. Chiang Y, Young D, Sladek J, Sladek V (2017) Local radial basis function collocation method for bending analyses of quasicrystal plates. Appl Math Model 50:463–483
4. Choi S, Chun M, Van Tyne C, Moon Y (2006) Optimization of open die forging of round shapes using FEM analysis. J Mater Process Technol 172(1):88–95
5. Cleary PW, Prakash M, Das R, Ha J (2012) Modelling of metal forging using SPH. Appl Math Model 36(8):3836–3855
6. Dadar N, Hematiyan M, Khosravifard A, Shiah Y (2020) An inverse meshfree thermoelastic analysis for identification of temperature-dependent thermal and mechanical material properties. J Therm Stress 43(9):1165–1188
7. Dai K, Liu G, Han X, Lim K (2005) Thermomechanical analysis of functionally graded material (FGM) plates using element-free Galerkin method. Comput Struct 83(17–18):1487–1502
8. Damaziak K, Malachowski J (2019) Comparison of SPH and FEM in thermomechanical coupled problems. In: AIP conference proceedings, AIP Publishing LLC, 2078:020063
9. De Bona F, Benasciutti D, Moro L, Novak JS (2019) FEM strategies for large scale thermo-mechanical simulations with material Non-linearity. In: IOP conference series: materials science and engineering, IOP Publishing, vol 649, p 012022
10. Debbabi I, BelhadjSalah H (2018) Analysis of thermo-elastic problems using the improved element-free Galerkin method. Comput Appl Math 37:1379–1394
11. Deng D (2009) FEM prediction of welding residual stress and distortion in carbon steel considering phase transformation effects. Mater Des 30:359–366
12. Desmorat R, Kane A, Seyedi M, Sermage JP (2007) Two scale damage model and related numerical issues for thermo-mechanical high cycle fatigue. Eur J Mech A/Solids 26(6):909–935
13. Garg S, Pant M (2017) Numerical simulation of thermal fracture in functionally graded materials using element-free Galerkin method. Sādhanā 42(3):417–431
14. Gingold RA, Monaghan JJ (1977) Smoothed particle hydrodynamics: theory and applications to non-spherical stars. Mon Not R Astron Soc 181:375–389
15. Hanoglu U, Sarler B (2013) Local radial basis function collocation method for solving thermo-mechanics of hot shape rolling of steel. In: COUPLED V: proceedings of the V international conference on computational methods for coupled problems in science and engineering, CIMNE, pp 116–126
16. Hanoglu U, Šarler B (2018) Multi-pass hot-rolling simulation using a meshless method. Comput Struct 194:1–14
17. Hanoglu U, Šarler B (2019) Hot rolling simulation system for steel based on advanced meshless solution. Metals 9:788
18. Hanoglu U, Sarler B et al (2011) Thermo-mechanical analysis of hot shape rolling of steel by a meshless method. Procedia Eng 10:3173–3178
19. Hasanpour K, Mirzaei D (2018) A fast meshfree technique for the coupled thermoelasticity problem. Acta Mech 229(6):2657–2673
20. Hong Y, Lin J, Chen W (2019) Simulation of thermal field in mass concrete structures with cooling pipes by the localized radial basis function collocation method. Int J Heat Mass Transf 129:449–459
21. Jaberzadeh E, Azhari M, Boroomand B (2013) Thermal buckling of functionally graded skew and trapezoidal plates with different boundary conditions using the element-free galerkin method. Eur J Mech A/Solids 42:18–26
22. Jaśkowiec J, Milewski S (2016) Coupling finite element method with meshless finite difference method in thermomechanical problems. Comput Math Appl 72(9):2259–2279
23. Khosravifard A, Hematiyan M, Ghiasi N (2020) A meshfree method with dynamic node reconfiguration for analysis of thermoelastic problems with moving concentrated heat sources. Appl Math Model 79:624–638
24. Koric S, Hibbeler LC, Thomas BG (2009) Explicit coupled thermo-mechanical finite element model of steel solidification. Int J Numer Methods Eng 78(1):1–31
25. Kosec G, Slak J, Depolli M, Trobec R, Pereira K, Tomar S, Jacquemin T, Bordas SP, Wahab MA (2019) Weak and strong from meshless methods for linear elastic problem under fretting contact conditions. Tribol Int 138:392–402
26. Kuhnert J (1999) General smoothed particle hydrodynamics. Ph.D. Thesis, Technische Universität Kaiserslautern
27. Liu GR (2009) Mesh free methods: moving beyond the finite element method, 2nd edn. CRC Press, Boca Raton
28. Lucy LB (1977) A numerical approach to the testing of the fission hypothesis. Astron J 82:1013–1024
29. Mavrič B, Šarler B (2015) Local radial basis function collocation method for linear thermoelasticity in two dimensions. Int J Numer Methods Heat Fluid Flow 25(6):1488–1510
30. Mavrič B, Šarler B (2017) Application of the RBF collocation method to transient coupled thermoelasticity. Int J Numer Methods Heat Fluid Flow 27(5):1064–1077
31. Memari A, Azar MRK (2019) Thermo-mechanical shock fracture analysis by meshless method. Theoret Appl Fract Mech 102:171–192
32. Moarrefzadeh A, Shahrooi S, Azizpour MJ (2019) The application of the meshless local Petrov–Galerkin method for the analysis of heat conduction and residual stress due to welding. Int J Adv Manuf Technol 104(1–4):723–742
33. Neto D, Martins J, Cunha P, Alves J, Oliveira M, Laurent H, Menezes L (2018) Thermo-mechanical finite element analysis of the AA5086 alloy under warm forming conditions. Int J Solids Struct 151:99–117
34. Nguyen NT, Bui TQ, Nguyen MN, Truong TT (2020) Meshfree thermomechanical crack growth simulations with new numerical integration scheme. Eng Fract Mech 235:107121
35. Oñate E, Perazzo F, Miquel J (2001) A finite point method for elasicity problem. Comput Struct 79:2151–2163
36. Pant M, Singh I, Mishra B (2011) A numerical study of crack interactions under thermo-mechanical load using EFGM. J Mech Sci Technol 25(2):403–413
37. Reséndiz-Flores EO, Saucedo-Zendejo FR (2015) Two-dimensional numerical simulation of heat transfer with moving heat source in welding using the finite pointset method. Int J Heat Mass Transf 90:239–245
38. Reséndiz-Flores EO, Saucedo-Zendejo FR (2018) Numerical simulation of coupled fluid flow and heat transfer with phase change using the finite pointset method. Int J Therm Sci 133:13–21
39. Rodriguez J, Carbonell JM, Cante J, Oliver J (2016) The particle finite element method (PFEM) in thermo-mechanical problems. Int J Numer Methods Eng 107(9):733–785
40. Rodríguez J, Jonsén P, Svoboda A (2017) Simulation of metal cutting using the particle finite-element method and a physically based plasticity model. Comput Part Mech 4(1):35–51
41. Rodríguez J, Carbonell J, Jonsen P (2020) Numerical methods for the modelling of chip formation. Arch Comput Methods Eng 27(2):387–412
42. Saucedo-Zendejo FR, Reséndiz-Flores EO (2020) Meshfree numerical approach based on the Finite Pointset Method for static linear elasticity problems. Comput Methods Appl Mech Eng 372:113367
43. Singh S, Singh J, Shukla K (2013) Buckling of laminated composite plates subjected to mechanical and thermal loads using meshless collocations. J Mech Sci Technol 27(2):327–336
44. Slak J, Kosec G (2019) Refined meshless local strong form solution of Cauchy–Navier equation on an irregular domain. Eng Anal Bounda Elem 100:3–13
45. Suchde P, Kuhnert J (2019) A fully lagrangian meshfree framework for PDEs on evolving surfaces. J Comput Phys 395:38–59

46. Talebi H, Frönd M, dos Santos JF, Klusemann B (2017) Thermomechanical simulation of friction stir welding of aluminum using an adaptive element-free Galerkin method. Pamm 17(1):473–474
47. Tiwari S, Kuhnert J (2002) A meshfree method for incompressible fluid flows with incorporated surface tension. Revue Eur Elem 11(7–8):965–987
48. Tiwari S, Kuhnert J (2007) Modeling of two-phase flows with surface tension by finite pointset method (FPM). J Comput Appl Math 203:376–386
49. Wu C, Hu W, Wang HP (2015) Lu H (2015) A robust numerical procedure for the thermomechanical flow simulation of friction stir welding process using an adaptive element-free Galerkin method. Math Probl Eng 2015:1–16
50. Yu S, Peng M, Cheng H, Cheng Y (2019) The improved element-free Galerkin method for three-dimensional elastoplasticity problems. Eng Anal Bound Elem 104:215–224
51. Zander N, Kollmannsberger S, Ruess M, Yosibash Z, Ranka E (2012) The finite cell method for linear thermoelasticity. Comput Math Appl 64:3527–3541
52. Zhang JP, Wang SS, Gong SG, Zuo QS, Hu HY (2019) Thermomechanical coupling analysis of the orthotropic structures by using element-free Galerkin method. Eng Anal Bound Elem 101:198–213

Publisher's Note Springer Nature remains neutral with regard to jurisdictional claims in published maps and institutional affiliations.